

Supporting Information

Experimental charge density distribution of non-coordinating sp³ carbanions in [Mg{(pz*)₃C}]₂

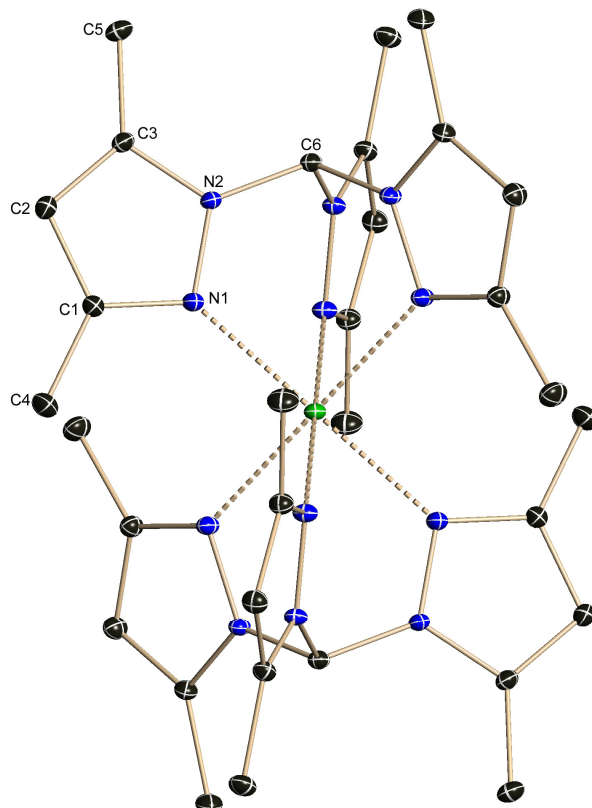
Daniel Kratzert,^a Dirk Leusser,^a Daniel Stern,^a Jens Meyer,^b Frank Breher,^b and Dietmar Stalke^{*a}

^a Institut für Anorganische Chemie der Universität Göttingen Tammannstraße 4, 37077 Göttingen, Germany, FAX: int. (+49)551-39-3459, E-mail: dstalke@chemie.uni-goettingen.de

^b Institut für Anorganische Chemie der Universität Karlsruhe, Engesserstraße 15, 76131 Karlsruhe, Germany

This PDF file includes:

- 1 X-ray investigation
- 2 Multipole Refinement
- 3 References



1 X-ray investigation of 1

The high-resolution data for the multipole refinement were collected from an oil-coated shock-cooled crystal on a BRUKER TXS diffractometer with D8 goniometer and INCOATEC Helios mirror optics (Mo-K α radiation, $\lambda = 0.71073 \text{ \AA}$) equipped with an Oxford Helijet open stream liquid helium cooling device and an APEXII detector.

The data were collected with omega-scans ($\Delta\omega = 0.3^\circ$) at fixed φ -angles with a detector distance of 5 cm at exposure times between 2 (low-order) and 40s (high-order data). This procedure led to a high-resolution data set (for details see Table S1), which was corrected for absorption, scaled and merged with SADABS-2008/2¹.

The data were integrated with SAINT². The structure was solved by direct methods (SHELXS)³ and refined by full-matrix least squares methods against F^2 (SHELXL-97).³ The refined independent atom model (IAM) served as the starting model for the subsequent multipole refinement. The following strategy to obtain the starting model was applied: the positional and anisotropic displacement parameters of the non-hydrogen atoms were refined with the high-order data ($d_{\max} = 0.52 \text{ \AA}$). The resulting positional and anisotropic displacement parameters were kept fixed during the subsequent refinement steps.

The hydrogen atoms were identified by a difference Fourier analysis using the low-order data ($d_{\min} = 0.98 \text{ \AA}$). Then the hydrogen atoms were shifted along their bonding vectors to distances of 1.085 \AA for those bound to sp³-hybridized carbon atoms and 1.076 \AA for those bound to sp²-hybridized carbon atoms, respectively. The hydrogen atoms at C4 showed a rotational disorder which could be modulated successfully. The identification of the second part of the disorder was not possible by difference Fourier analysis. Instead the two parts of the disorder were modeled by AFIX 137 in two parts. The occupation factors refined to 0.695 and 0.305 and were fixed during the subsequent refinements to 0.7 and 0.3, respectively.

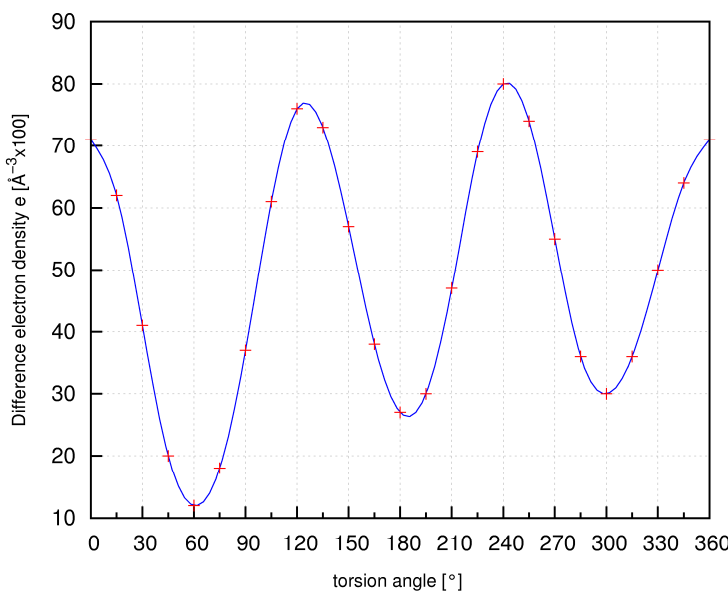


Figure 1 Difference electron density at the cone around C4.

Crystal data for **1**: $C_{38}H_{42}MgN_{12}$, $M = 691.15$ g/mol, rhombohedral space group $R\bar{3}$, $a = 10.637(2)$, $b = 10.637(2)$, $c = 24.594(5)$ Å, $V = 2409.8(9)$ Å³, $Z = 3$, $\rho_{\text{calc.}} = 1.429$ Mg/m³, $\mu = 0.107$ mm⁻¹, 65508 reflections measured, 5725 independent, $R1(I > 2\sigma(I)) = 0.0291$, $wR2(I > 2\sigma(I)) = 0.0972$. Multipole refinement of **1**: $R(F^2) = 0.016$, $R_w(F^2) = 0.035$, GoF = 2.502. Crystallographic data (excluding structure factors) for the structures reported in this paper have been deposited with the Cambridge Crystallographic Data Centre as supplementary publication no 793609. Copies of the data can be obtained free of charge on application to CCDC, 12 Union Road, Cambridge CB2 1EZ, UK [fax: (internat.) + 44(1223)336-033; e-mail: deposit@ccdc.cam.ac.uk].

2 Multipole Refinement

The multipole refinement using the atom-centered multipole model of Hansen and Coppens⁴ was carried out on F^2 with the full-matrix-least-squares refinement program XDLSM implemented in the XD2006⁵ program package. Preliminary tested models led to a flat and featureless residual density distribution except a residual density peak at the Magnesium atom position. The appearance of this peak presumably originates from the very restricted definition of poles at the special position of the magnesium atom. It seems that the restrictions of the crystallographic symmetry are in conflict with the local symmetry of the multipoles.

The core and the spherical valence densities were composed of relativistic Dirac-Fock wave functions reported by Su, Coppens and Macchi (SCM bank file).⁶ The radial fit of these functions was optimized by refinement of the expansion-contraction

parameters κ and κ' . The expansions over the spherical harmonics were truncated at the hexadecapolar level for all hetero atoms and all multipoles ($n_l = 1$ to 4) of each atom shared the same κ' -set (*keep kappa* constraint). The deformation densities of the hydrogen atoms were represented by bond directed dipoles and quadrupoles. To derive adequate parameters for the contraction of the hydrogen atoms, κ and κ' values suggested by Volkov *et al.* were introduced and kept fixed during the refinement.⁷ Moreover, a riding model and distance constraints were applied for the hydrogen atoms during the first steps of the multipole refinement. In the final steps of the refinement the hydrogen atoms (except the disordered group at C4) were refined without distance and thermal motion constraints by using a low-order cut-off. After each step the change of the hydrogen parameters was checked for significance.

Several models have been refined and compared, differing in the degree of applied chemical constraints and local non-crystallographic symmetry. A maximum amount of chemical constraints and symmetry restrictions for the multipolar functions stabilized the refinement procedures in the non-centrosymmetric space group and reduced correlations. On the other hand the model had to be flexible enough to account for small differences of supposed chemically equivalent atoms. The density parameters were implemented in the refinement routines in a stepwise manner but in the final cycles all parameters but the κ' (due to the known effect of large correlations with the other multipole parameters) were refined together using all positive reflections (no $\parallel\sigma$ exclusion to avoid bias) until convergence was reached. Chemically equivalent or similar atoms were constrained to share the same expansion/contraction parameters, monopole and multipole populations in the beginning of the refinement. In the final refinement stages all constraints for similar atoms were dismissed.

Hydrogen atoms with similar chemical environment were modeled with one set of parameters each. The hydrogen atoms H4B and H4C were chemically constrained to H4A, H4E and H4F where constrained to H4D. Also H5B and H5C were constrained to H5A. Due to the diffuse density around C4 the free refinement of the adjacent hydrogen atoms was not possible. They were kept as a rigid group which was able to move with C4.

The multipole refinement led to a very satisfactory fit. The electron density is not biased by and well separated from the thermal motion of the non-hydrogen atoms. This was justified by the rigid bond test (DMSDA test) according to Hirshfeldt.⁸

2.1 Results of the DMSDA-test

Differences of Mean-Squares
Displacement Amplitudes (DMSDA)
[10^4 \AA^2] along interatomic bonds [\AA]

N1–N2	1.3755	-2
N2–C3	1.3532	2
C1–C2	1.4076	0
C2–C3	1.3865	-1
C4–C5	1.4869	6
N1–C1	1.3359	2
N2–C6	1.4421	6
C1–C4	1.4918	3

2.2 Residuals

The final model which included just those constraints that were chemically sensible led to the lowest R -values and a flat and featureless residual density. Therefore, this model was selected for the subsequent discussion.

The final residuals were:

$$R(F) = 0.0189, R_{\text{w}}(F) = 0.0180, R(F^2) = 0.0213, R_{\text{w}}(F^2) = 0.0343$$

$$\text{GOF}_w = 2.476 / \text{GOF} = 2.476$$

$$N_{\text{reflections}}/N_{\text{variables}} = 23.4 \text{ in the final cycle}$$

The final parameters of the multipole model (populations, contraction/expansion parameters) can be found in the CIF-file.

Table S1. Crystal data of 1.

Empirical formula	C38 H42 Mg N12		
Formula weight	691.15		
Temperature [K]	15(1)		
Wavelength [\text{\AA}]	0.71073		
Crystal system	rhombohedral		
Space group	$R\bar{3}$		
Unit cell dimensions [\text{\AA}]	$a = 10.633(1)$	$\alpha = 90^\circ$	
	$b = 10.633(1)$	$\beta = 90^\circ$	
	$c = 24.569(2)$	$\gamma = 120^\circ$	
Volume [\text{\AA}^3]	2405.5(9)		

Z	3
Density (calculated) [Mg/m ³]	1.429
Absorption coefficient [mm ⁻¹]	0.107
F(000)	1098
Crystal size [mm]	0.13 x 0.24 x 0.25
Theta range for data collection [°]	2.48 – 50.46
Index ranges	-23<=h<=23, -23<=k<=22, -53<=l<=53
Reflections collected	65508
Independent reflections	5725
Completeness to theta = 50.46°	99.9
Absorption correction	empirical
Max. and min. transmission	0.9361, 1.0000
Refinement method	Full-matrix least-squares on F^2
Data / parameters	5577 / 248
wGoF on F^2 , GoF on F^2	2.476, 2.476
Final R indices based on all data	$R\{F\} = 0.0189$ $Rw\{F\} = 0.0180$ $R\{F^2\} = 0.0213$ $Rw\{F^2\} = 0.0343$
Largest diff. peak and hole [e/ Å ³]	0.286, -0.154

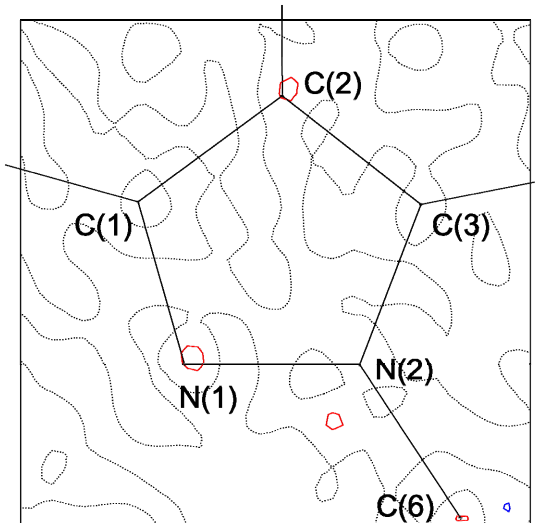
2.3 Bond Lengths [Å] and Angles [°]

N(1)–N(2)	1.3755(2)	N(2)–N(1)–C(1)	105.971(17)	H(4A)–C(4)–H(4B)	109.480376(0)
N(1)–C(1)	1.3359(3)	N(1)–N(2)–C(3)	110.941(18)	H(4A)–C(4)–H(4C)	109.475933(0)
N(2)–C(3)	1.3532(2)	N(1)–N(2)–C(6)	123.443(19)	H(4A)–C(4)–H(4D)	134.710806(0)
N(2)–C(6)	1.4421(2)	N(1)–N(2)–C(6)	123.444(19)	H(4A)–C(4)–H(4E)	34.262317(0)
N(2)–C(6)	1.4420(2)	N(1)–N(2)–C(6)	123.444(19)	H(4A)–C(4)–H(4F)	77.879056(0)
N(2)–C(6)	1.4421(2)	C(3)–N(2)–C(6)	125.609(19)	H(4B)–C(4)–H(4C)	109.474505(0)
C(1)–C(2)	1.4076(3)	C(3)–N(2)–C(6)	125.608(19)	H(4B)–C(4)–H(4D)	77.864064(0)
C(1)–C(4)	1.4918(3)	C(3)–N(2)–C(6)	125.608(19)	H(4B)–C(4)–H(4E)	134.720564(0)
C(2)–C(3)	1.3865(3)	C(6)–N(2)–C(6)	0.001818(1)	H(4B)–C(4)–H(4F)	34.247484(0)
C(2)–H(2)	1.075604(0)	C(6)–N(2)–C(6)	0.004119(1)	H(4C)–C(4)–H(4D)	34.254704(0)
C(3)–C(5)	1.4869(3)	C(6)–N(2)–C(6)	0.003096(0)	H(4C)–C(4)–H(4E)	77.859772(0)
C(4)–H(4A)	1.084232(0)	N(1)–C(1)–C(2)	110.318(18)	H(4C)–C(4)–H(4F)	134.709174(0)
C(4)–H(4B)	1.084585(0)	N(1)–C(1)–C(4)	121.541(17)	H(4D)–C(4)–H(4E)	109.468630(0)
C(4)–H(4C)	1.084588(0)	C(2)–C(1)–C(4)	128.137(17)	H(4D)–C(4)–H(4F)	109.466901(0)
C(4)–H(4D)	1.084597(0)	C(1)–C(2)–C(3)	105.695(17)	H(4E)–C(4)–H(4F)	109.494254(0)
C(4)–H(4E)	1.084348(0)	C(1)–C(2)–H(2)	126.101(11)	C(3)–C(5)–H(5A)	111.092(9)
C(4)–H(4F)	1.084543(0)	C(3)–C(2)–H(2)	128.203(12)	C(3)–C(5)–H(5B)	108.900(9)
C(5)–H(5A)	1.084606(0)	N(2)–C(3)–C(2)	107.059(17)	C(3)–C(5)–H(5C)	111.396(10)
C(5)–H(5B)	1.084407(0)	N(2)–C(3)–C(5)	122.039(17)	H(5A)–C(5)–H(5B)	110.500789(0)
C(5)–H(5C)	1.084411(0)	C(2)–C(3)–C(5)	130.862(17)	H(5A)–C(5)–H(5C)	106.346818(0)
H(4A)–H(4E)	0.638777(0)	C(1)–C(4)–H(4A)	109.434(10)	H(5B)–C(5)–H(5C)	108.564565(0)
H(4B)–H(4F)	0.638670(0)	C(1)–C(4)–H(4B)	109.460(10)	N(2)–C(6)–N(2)	109.097(14)
H(4C)–H(4D)	0.638818(0)	C(1)–C(4)–H(4C)	109.502(10)	N(2)–C(6)–N(2)	109.101(14)
		C(1)–C(4)–H(4D)	109.507(10)	N(2)–C(6)–N(2)	109.102(14)
		C(1)–C(4)–H(4E)	109.454(10)	C(4)–H(4A)–H(4E)	72.878780(0)
		C(1)–C(4)–H(4F)	109.437(10)	C(4)–H(4B)–H(4F)	72.872659(0)
				C(4)–H(4C)–H(4D)	72.873454(0)
				C(4)–H(4D)–H(4C)	72.871844(0)
				C(4)–H(4E)–H(4A)	72.858905(0)
				C(4)–H(4F)–H(4B)	72.879859(0)

2.4 Residual Density Distribution

Results from the Fast Fourier Transformation (XDFFT):

diff_density_max: 0.286 e \AA^{-3}
diff_density_min: -0.154 e \AA^{-3}
diff_density_rms: 0.031 e \AA^{-3}
highest peaks: Q1 = 0.29, Q2 = 0.21 e \AA^{-3}



residual density in the p_z^* -ring plane
(all data, contour interval = 0.1 e \AA^{-3})

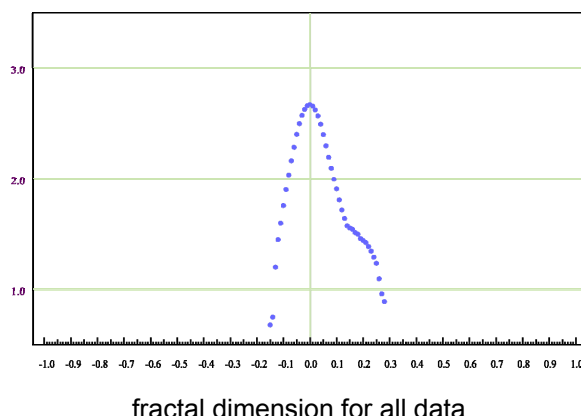


Figure S2: Residual density analysis of 1

The residual density is in very good approximation flat and featureless, which can be seen by visual inspection of the Fourier maps above or numerically by jnk2RDA developed by K. Meindl and J. Henn.⁹ The shape of the distribution of the fractal dimension shows a shoulder on very low level (< 0.3 e \AA^{-3}) because of the residual density near the Magnesium atom.

2.5 Bond Critical Points (BCPs)

Table S2. Topological parameters of the bond critical points and integrated atomic charges with esds calculated from XDPROP; the esds for the averaged values were calculated from the minimum and maximum deviation from the mean value.

bond	$\rho(\mathbf{r}_{\text{BCP}})$	$\nabla^2\rho(\mathbf{r}_{\text{BCP}})$	BP	d1	d2	λ_1	λ_2	λ_3	$\varepsilon(\mathbf{r}_{\text{BCP}})$
MG(1)-N(1)	0.208	3.327	2.1973	0.9402	1.2571	-1.45	-1.28	6.06	0.14
N(2)-C(6)	1.792	-15.033	1.4422	0.8629	0.5793	-15.33	-11.84	12.14	0.29
N(2)-N(1)	2.335	-5.633	1.3755	0.6997	0.6758	-19.88	-17.71	31.96	0.12
N(2)-C(3)	2.286	-21.501	1.3534	0.8006	0.5528	-19.77	-16.65	14.92	0.19
C(3)-C(5)	1.806	-14.591	1.4871	0.7612	0.7259	-12.84	-12.62	10.86	0.02
C(3)-C(2)	2.154	-17.775	1.3870	0.6959	0.6911	-17.38	-13.43	13.04	0.29
C(2)-C(1)	2.069	-16.483	1.4079	0.6932	0.7147	-15.69	-13.52	12.73	0.16
N(1)-C(1)	2.434	-23.221	1.3360	0.7688	0.5672	-21.23	-17.65	15.66	0.20
C(1)-C(4)	1.873	-12.922	1.4918	0.7389	0.7530	-12.91	-12.69	12.68	0.02
C(2)-H(2)	1.744	-17.079	1.0759	0.7373	0.3386	-16.97	-16.15	16.03	0.05
C(4)-H(4A)	2.336	-15.570	1.1849	0.6099	0.5751	-18.22	-8.10	10.75	1.25
C(4)-H(4B)	2.334	-15.553	1.1852	0.6098	0.5754	-18.22	-8.09	10.76	1.25
C(4)-H(4C)	2.333	-15.555	1.1852	0.6099	0.5753	-18.23	-8.09	10.76	1.25
C(4)-H(4D)	2.333	-15.555	1.1114	0.6099	0.5015	-18.23	-8.09	10.76	1.25
C(4)-H(4E)	2.336	-15.570	1.1111	0.6099	0.5013	-18.22	-8.10	10.75	1.25
C(4)-H(4F)	2.334	-15.553	1.1113	0.6098	0.5015	-18.22	-8.09	10.76	1.25
C(5)-H(5A)	1.715	-18.877	1.0846	0.7618	0.3228	-16.65	-16.02	13.79	0.04
C(5)-H(5B)	1.714	-18.829	1.0845	0.7619	0.3226	-16.59	-16.04	13.81	0.03
C(5)-H(5C)	1.714	-18.867	1.0844	0.7615	0.3229	-16.64	-16.01	13.78	0.04

λ_3 is the curvature of $\rho(\mathbf{r})$ along the bond path, the ellipticity $\varepsilon = \lambda_2/\lambda_1 - 1$, d_{BP} the total length of the BP, $d1_{\text{BCP}}$ the distance of the first named atom to the BCP.

2.6 Integrated charges

Atom	integrated atomic charge
Mg(1)	+1.840
N(1)	-0.618
N(2)	-0.733
C(1)	+0.334
C(2)	-0.1957
C(3)	+0.353
C(4)	-0.427
C(5)	-0.516
C(6)	+0.636
H(2)	+0.201
H(4A,B,C)	+0.166
H(5A)	+0.1900

All anticipated critical points could be determined and quantified. Presumably due to the disorder, the bond path between C4 and H4A-C could not be found. Instead a highly curved BP between C4 and H4D-F was found.

The bond critical points (BCP), (3, -1) critical points in $\rho(\mathbf{r})$, are displayed as red spheres.

The ring critical point, (3, +1) critical points in $\rho(\mathbf{r})$, are displayed as yellow spheres.

The connection lines between the atoms are the calculated bond paths (BP), lines of maximum density between two atoms with respect to any neighbouring line. The atoms are represented as blue spheres, (3, +3) critical points (local maxima).

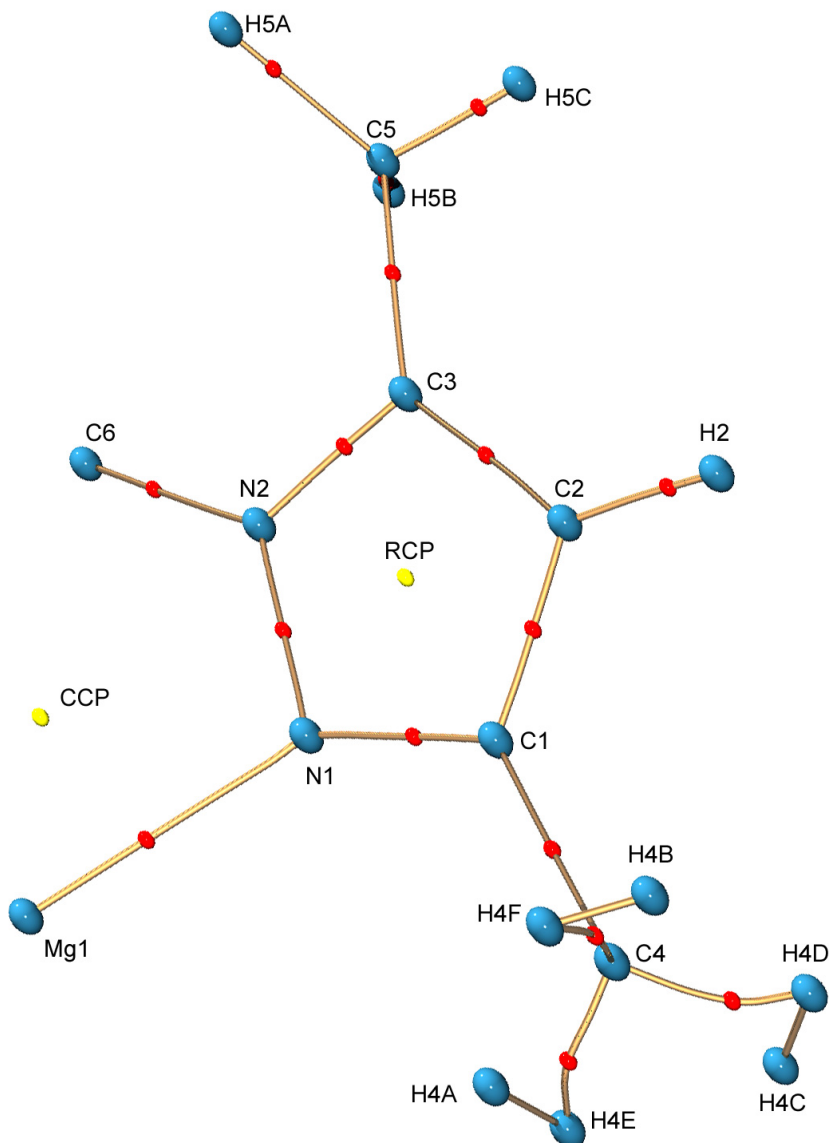
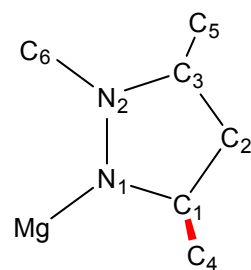
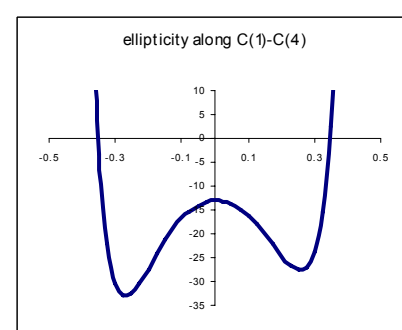
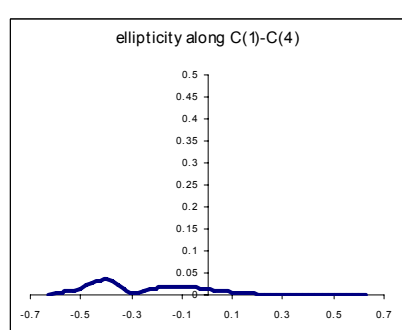
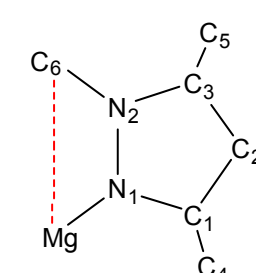
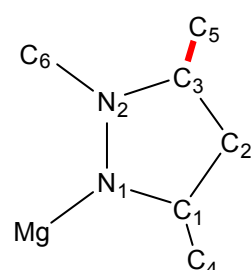
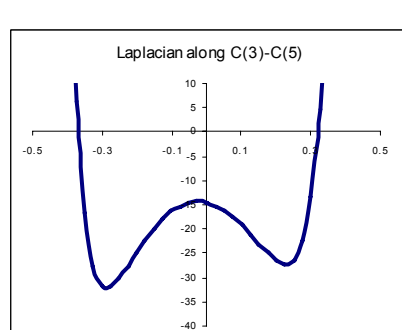
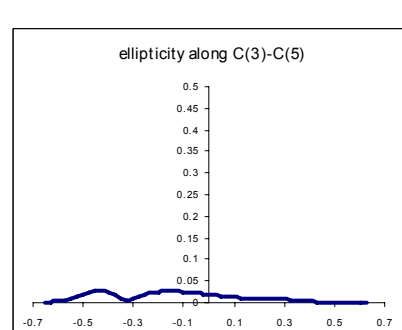
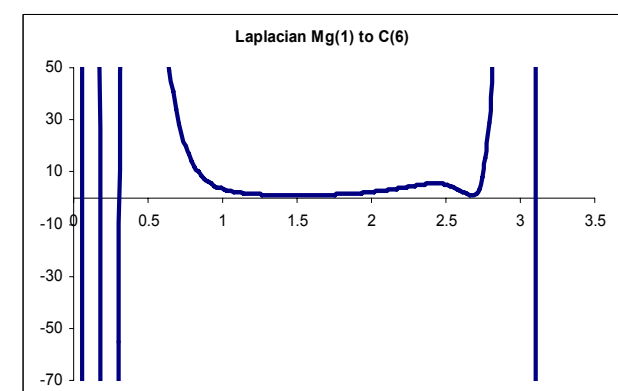
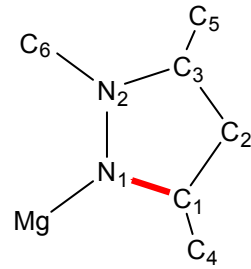
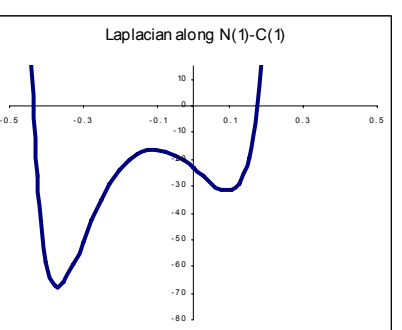
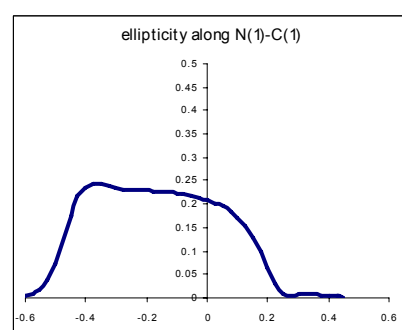
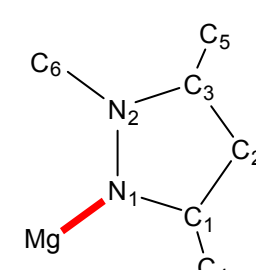
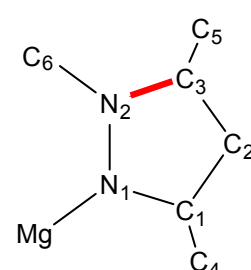
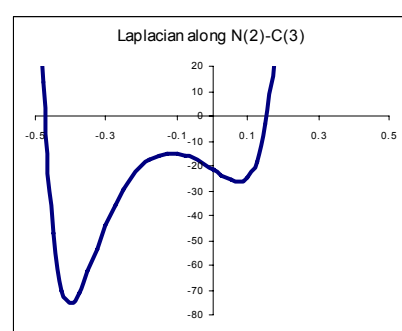
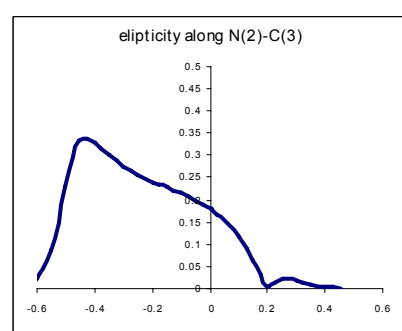
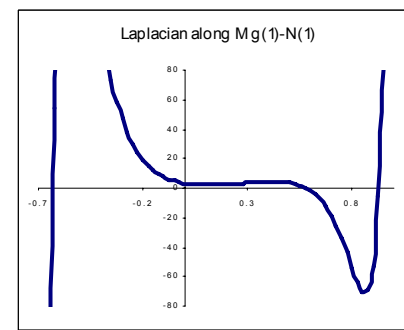
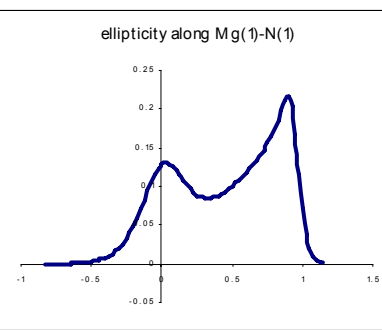
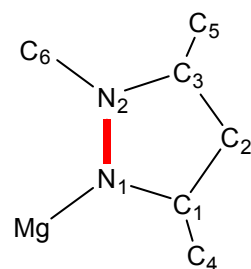
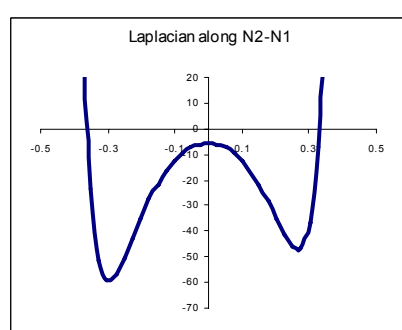
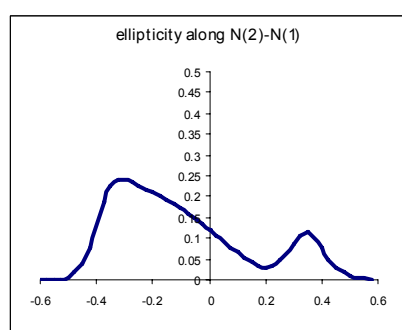
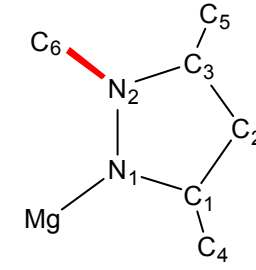
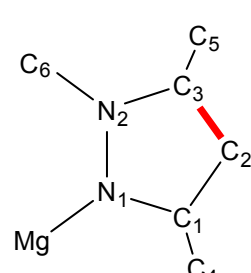
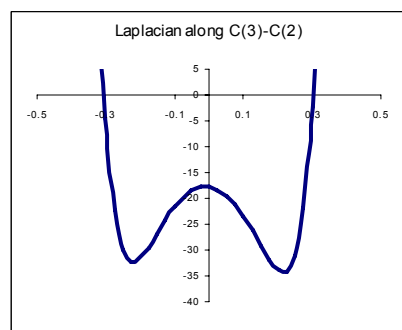
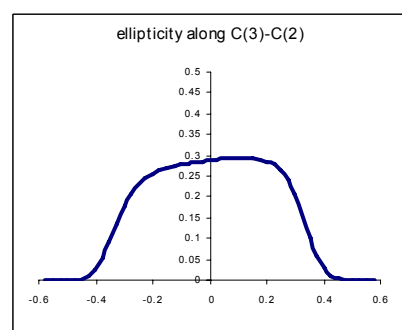
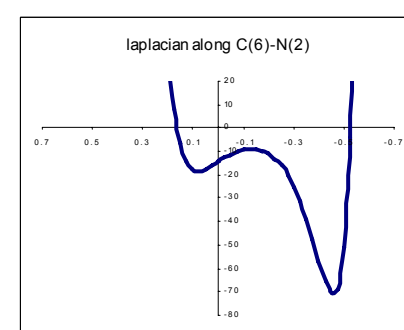
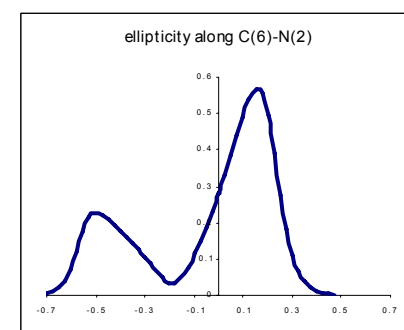
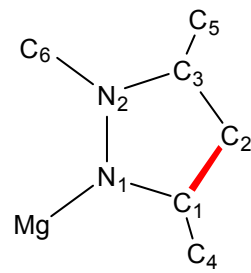
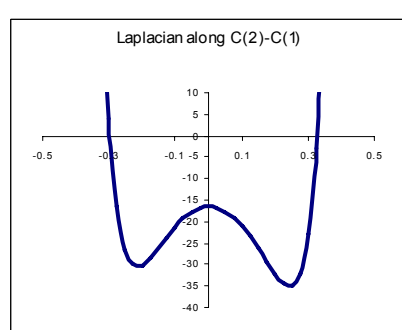
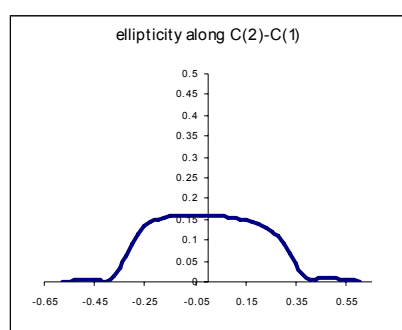


Figure S3: Molecular graph of 1, made up by the bond paths (BP, connection lines), bond critical points (BCP, red spheres), ring critical points (yellow spheres), and local extrema of the density (atomic positions, blue spheres).

2.7 Bond Path Analysis

The plotted properties are the ellipticity $\epsilon(\mathbf{r})$ (left) and the Laplacian $L(\mathbf{r}) [\text{e}\text{\AA}^{-5}]$ (right) along the bond path (BP) from the first to the second labelled atom. The y-axis (property) intersects the x-axis (distance from the bond critical point BCP [\AA]) at the BCP and therefore separates the BP into basins of the first (left) and the second labelled (right) atom.



2.8 Laplacian Distribution

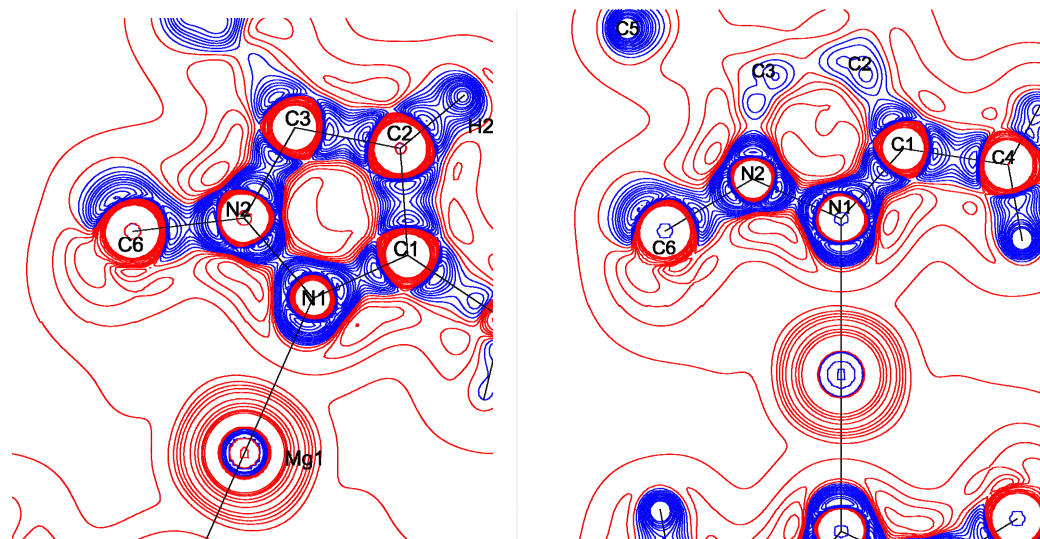


Figure S4 $L(r)$ in selected planes negative values ranging from -1 to $-100 \text{ e}\text{\AA}^{-5}$ (charge concentrations) are plotted in blue and positive values ranging from $+1$ to $+50 \text{ e}\text{\AA}^{-5}$ (charge depletions) in red contour lines.

2.9 Electrostatic Potential

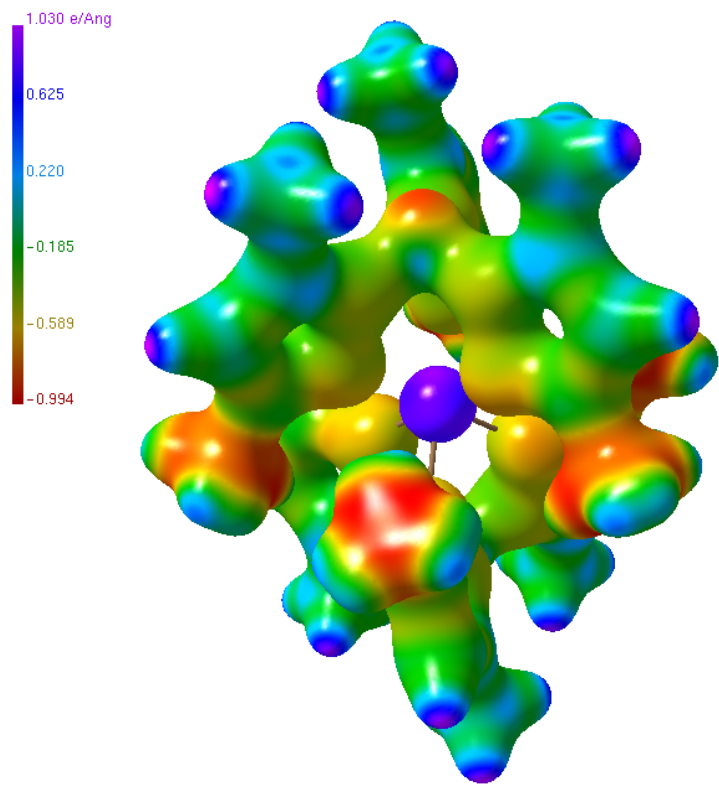


Figure S5: Electrostatic potential (color-coded) mapped on the isosurface representation of the electron density distribution on the $0.6 \text{ e}\text{\AA}^{-5}$ level.¹⁰

The electrostatic potential (ESP) mapped on an isosurface of the electron density distribution is a useful tool to identify attractive regions for nucleophiles or electrophiles, respectively. Nucleophiles tend to attack regions with positive potential (electron depletion, blue). Sites for preferred attack of electrophiles are those with negative potential (red). We locate the area with the highest values of positive ESP at the magnesium atom and the methyl group C5. The most distinct negative values at the C6 and the methyl group C4.

References

- 1 G. M. Sheldrick, *SADABS 2008/2*, (2008), Göttingen.
- 2 Bruker AXS Inc. *SAINT*, V7.68A (2010).
- 3 G. M. Sheldrick, *Acta Crystallogr., Sect. A.*, 2008, **64**, 112.
- 4 N. K. Hansen and P. Coppens, *Acta Crystallogr.*, 1978, **A34**, 909.
- 5 XD A. Volkov, P. Macchi, L. J. Farrugia, C. Gatti, P. R. Mallinson, T. Richter and T. Koritsanszky, *XD2006, A Computer Program Package for Multipole Refinement, Topological Analysis of Charge Densities and Evaluation of Intermolecular Energies from Experimental or Theoretical Structure Factors*, (2006).
- 6 Z. Su and P. Coppens, *Acta Crystallogr.*, 1998, **A54**, 646; P. Macchi and P. Coppens, *Acta Crystallogr.*, 2001, **A57**, 656.
- 7 A. Volkov, Y. A. Abramov and P. Coppens, *Acta Crystallogr., Sect. A.*, 2001, **57**, 272.
- 8 F. L. Hirshfeld, *Acta Crystallogr.*, 1976, **A32**, 239.
- 9 K. Meindl and J. Henn, *Acta Crystallogr., Sect. A.*, 2008, **64**, 404.
- 10 C. B. Hübschle and P. Luger, *J. Appl. Crystallogr.*, 2006, **39**, 901.